Supplementary Materials for:

Modular assembly of the nucleolar large subunit processome

Zahra Assur Sanghai[1,2], Linamarie Miller[1,2,3], Kelly R. Molloy[4], Jonas Barandun[2], Mirjam Hunziker[2], Malik Chaker-Margot[2,3], Junjie Wang[4], Brian T. Chait[4] and Sebastian Klinge[2]*

[1] equal contribution

[2] Laboratory of Protein and Nucleic Acid Chemistry, The Rockefeller University, New York, New York 10065, USA

[3] Tri-Institutional Training Program in Chemical Biology, The Rockefeller University, New York, New York 10065, USA

[4] Laboratory of Mass Spectrometry and Gaseous Ion Chemistry, The Rockefeller University, New York, New York 10065, USA.

* Correspondence should be addressed to S.K. (klinge@rockefeller.edu)

Materials and Methods

Purification of the large subunit processome

The large subunit processome was purified from a *Saccharomyces cerevisiae* BY4741 strain containing a TEV protease-cleavable C-terminal GFP tag on Nsa1 (Nsa1-linker-TEV-GFP) and a C-terminal 5 x beta-catenin 3C protease-cleavable tag on Nop2 (Nop2-linker-3C-Bc5), for endogenous expression. Cultures were grown in full synthetic drop-out (SD) media containing 2% raffinose (w/v) at 30 ºC to an optical density (OD) of 0.8-1, prior to addition of 2% galactose (w/v) for 16 hours, reaching saturation (OD 5-6). Cells were then harvested by centrifugation at 4000 x *g* for 10 minutes at 4 ºC. The cell pellet was washed with ice cold ddH_2O twice, followed by a wash with ddH_2O containing protease inhibitors (E64, Pepstatin, PMSF). Washed cells were immediately flash frozen in liquid nitrogen and lysed by 4 cycles of cryogenic grinding using a Retsch Planetary Ball Mill PM100.

The freshly ground yeast powder was resuspended by vortexing in buffer A (50 mM Tris-HCl, pH 7.6 (20 °C), 150 mM NaCl, 1 mM EDTA, 1 mM DTT, 0.1% Triton-X100, PMSF, Pepstatin, E-64), removing the insoluble fraction by centrifugation at 4 °C, 40,000 x *g* for 30 min. The supernatant was subsequently incubated with anti-GFP nanobody beads (Chromotek) for 3 hours at 4 °C, with agitation. The beads were washed four times in ice-cold buffer A before the bound proteins were eluted via TEV-protease cleavage (1 hour, 4 °C). The eluate was then incubated with NHS-sepharose beads (Sigma) coupled with anti-beta-catenin nanobody (*18*) in buffer B (50 mM Tris-HCl pH 7.6 (20 °C), 150 mM NaCl, 1 mM EDTA, 1 mM DTT) for 1 hour at 4 °C with agitation. For electron microscopy (EM) sample preparation, the anti-beta catenin beads were washed once with buffer B, before cleavage by 3C protease for 1 hour at 4 °C, releasing the Nsa1-Nop2 containing LSU processome. For protein-protein cross-linking analysis the eluate from GFP-nanobody beads was incubated with beta catenin-nanobody beads in buffer C (50 mM HEPES-NaOH pH 7.6 (4 °C), 150 mM NaCl, 1 mM EDTA) and eluted in the same buffer through 3C-protease cleavage. The eluted sample typically measured an absorbance at 260 nm (A260) of 2.4 to 4.5 mAU (Nanodrop 2000, Thermo Scientific) (fig. S1).

Cryo-EM sample and grid preparation

Cryo-EM grids were prepared on four different occasions for the 4 data sets obtained (ds1-ds4). The LSU processome eluate in sample buffer B (above) was left as is (ds1 only), or supplemented with 0.1% Triton X-100 and 5 mM $MgCl_2$ (final concentration, ds2-ds4). Copper grids of 400 mesh with lacey carbon and an ultra-thin carbon support film were used (Ted Pella Inc, product no. 01824) for data collection. A volume of 3 to 4 μl of LSU processome sample (A260 of 2.5) was applied onto glow-discharged grids and plunged into liquid ethane using a Vitrobot Mark IV robot (FEI Company) (100 % humidity, blot force of 0 and blot time 3.5-4 s).

Cryo-EM data collection and image processing

A total of 14,201 micrographs were obtained over four data collections (ds1 - ds4) on a Titan Krios (FEI Company), at 300 kV, with a K2 Summit detector (Gatan, Inc.). SerialEM (*19*) was employed for data acquisition using a defocus range of 1.0- 3.5 μm with a pixel size of 1.3 Å. Super-resolution movies with 32 frames were collected using a total dose of 10 electrons per pixel per second with an exposure time of 8 seconds and a total dose of 50 electrons per $Å^2$ (Table S1).

Upon data collection, the movies were gain corrected, dose weighted and aligned with Motioncor2 (*20*), and the contrast transfer function (CTF) was estimated using CTFFIND 4.1.5 (*21*). Relion 2.1 (*22*) was used for all subsequent particle picking, classifications and refinements. Corrected and aligned micrographs were first subjected to autopicking in Relion, resulting in a total of 1,653,290 selected particles from all 4 data sets. After manual inspection of all micrographs, particles were extracted with a box size of 480 pixels (2X-binned to 240 pixels), and 2D-classified separately for each individual data set. After 2D classification, bad classes were removed, and the selected particles of each data set were 3D-classified into four classes using an initial 3D model obtained from cryoSPARC (*23*), low-pass filtered to 60 Å. The best one to two classes from each 3D classification were selected and their particles were re-extracted with a box size of 480 pixels (un-binned). A combined total of 514,746 particles were finally used for 3D auto-refinement and post-processing with a solvent mask around the “core” containing

domains I and II of the 25S rRNA, resulting in an overall resolution of 3.4 Å for state 1 (fig. S2). A subsequent round of 3D classification without image alignment of these particles into 6 classes, was used to obtain the two classes that contained states 2 and 3 at 39% and 41% respectively of the total particles. A refinement of the class containing state 2 (201,114 particles) was performed using a mask to include the additional visible densities, comprising of domain VI and its associated proteins, to obtain a final map at 3.7 Å (fig. S2). By conducting an additional round of focused 3D classification without image alignment on this class with a mask around Mak11 and the neighboring segment of domain V of the 25S rRNA, a subset of particles emerged with improved density. This was refined to provide a more continuous map of Mak11 and domain V (state 2A) (fig. S2).Due to particle heterogeneity in the initial class containing state 3 (211,534 particles), a focused classification without image alignment of that class of particles was performed using a mask around the additional density containing domain III of the 25S rRNA, Erb1-CTD (WD40) and Ytm1 (WD40). The best class from this round of classification (31,419 particles) was refined with a mask around the entirety of state 3, to obtain a final map at 4.6 Å resolution. The local resolution of the maps were calculated using Resmap (*24*) (fig. S3).

Model building and refinement

By using the structure of the late nuclear LSU processome, Nog2-particle (PDB 3JCT,(*2*)) as reference, common assembly factors and ribosomal proteins were manually located and fitted into the density, using Cic1 and Rpl7 as hallmark anchors. Protein-protein interactions were confirmed by crosslinking and mass spectrometry analyses (described below). New assembly factors Mak16, Rrp1, Nop16, Erb1-NTD, Rrp14, Rrp15 and Ebp2 and segments of rRNA were modeled *de novo*. Previously determined crystal structures of assembly factors Nsa1 (PDB 5SUI) (*25*), Ytm1, Erb1-CTD (PDB 5CXB) (*26*) were docked and manually adjusted. Has1, Ssf1, Brx1, Rpf1 and Mak11 were docked from Phyre2 models initially and adjusted to fit the density (*27*). Model building was performed with COOT (*28*). An annotated list of individual protein IDs, reference models and corresponding maps used for building, can be found in Table S2. The model was refined against a half-map1 from the overall 3.7 Å map of state 2 in PHENIX with

phenix.real_space_refine using secondary structure restraints for proteins and RNAs (*29*). Refinement and model statistics can be found in Table S1.

Map and model visualization

All map and model analyses and illustrations were made using Chimera (*30*) and PyMOL Molecular Graphics System, Version 1.8 Schrödinger, LLC. Density map visualization for certain figures was also performed on UCSF ChimeraX, developed by the Resource for Biocomputing, Visualization, and Informatics and the University of California, San Francisco (supported by NIGMS P41-GM103311) (Goddard, 2017).

RNA extraction and Northern blotting

The *S. cerevisiae* large subunit processome *(*Nsa1/Nop2 particle) was purified as described above and RNA was extracted from the final 3C protease elution with 1 mL TRIzol (Life Technologies) according to the manufacturer's instructions. 1.0 µg of isolated Nsa1 particle RNA was separated on a denaturing 1.2% Formaldehyde-Agarose gel (SeaKem LE, Lonza) or a denaturing 10% Urea-PAGE (Fisher, Amresco). After staining the gel in 1X SYBR Green II (Lonza) ddH_2O solution (pH 7.5) for 30 min, RNA species were visualized with a Gel Doc EZ Imager (Bio-Rad) (fig. S1) and then transferred onto a cationized nylon membrane (Zeta-Probe GT, Bio-Rad) using downward capillary transfer in case of the agarose gel and a Trans Blot SD semi-dry transfer cell (Bio-Rad) for the Urea-PAGE gel. RNA was cross-linked to the membrane for Northern blot analysis by UV irradiation at 254 nm with a total exposure of 120 milli- joules/cm^2 in a UV Stratalinker 2400 (Stratagene). Cross-linked membranes were incubated with hybridization buffer (750 mM NaCl, 75 mM trisodium citrate, 1% (w/v) SDS, 10% (w/v) dextran sulfate, 25% (v/v) formamide) at 65°C for 30 min prior to addition of γ-^{32}P-end-labeled DNA oligo nucleotide probes. Used oligonucleotide probe sequences are as follows:

25S (TTTCACTCTCTTTTCAAAGTTCTTTTCATCT),
the ITS1 3' end (TTAATATTTTAAAATTTCCAG),
the ITS2 C2 site (TGGTAAAACCTAAAACGACCGT),
the 3' ETS 5' end (CCACTTAGAAAGAAATAAAAA),
and the 5S (CTACTCGGTCAGGCTC).

Probes were hybridized for 1 hour at 65 °C and then overnight at 37 °C. Membranes were washed once with wash buffer 1 (300 mM NaCl, 30 mM trisodium citrate, 1% (w/v) SDS) and once with wash buffer 2 (30 mM NaCl, 3 mM trisodium citrate, 1% (w/v) SDS) for 20 min each at 45°C. Radioactive signal was detected by exposure of the washed membranes to a storage phosphor screen which was scanned with a Typhoon 9400 variable-mode imager (GE Healthcare).

DSS cross-linking sample preparation and mass spectrometry analysis

The tandem-affinity purified LSU processome (Nsa1/Nog2-particle), eluted off anti-beta catenin nanobody beads (in 50 mM HEPES-NaOH pH 7.6 (4 °C), 150 mM NaCl, 1 mM EDTA, 1 mM DTT) at an absorbance of 1.0 at 260 nm (Nanodrop 2000, Thermo Scientific) were pooled (total volume 300 µl) and split into three 100 µl cross-linking reaction aliquots.

To each aliquot, 8.8 µl of Disuccinimidylsuberate (DSS; 25 mM in DMSO, Creative Molecules Inc.) was added to yield a final DSS concentration of 2.0 mM and samples were cross-linked for 30 minutes at 25 °C with 450 rpm constant mixing. The reactions were quenched with 50 mM ammonium bicarbonate (final concentration) and precipitated by adding methanol (Alfa Aesar, LC-MS grade) to a final concentration of 90% followed by incubation at -80 °C overnight. Precipitated cross-linked LSU processomes were combined into one tube by repeated centrifugation at 21,000 x *g*, 4 °C for 30 minutes. The resulting pellet was washed three times with 1 ml cold 90% methanol, air-dried and finally resuspended in 50 µl of 1X NuPAGE LDS buffer (Thermo Fisher Scientific).

DSS cross-linked samples were processed as in (*17*), and as described below. DSS cross-linked LSU processomes in LDS buffer were reduced with 25 mM DTT, alkylated with 100 mM 2-chloroacetamide, separated by SDS-PAGE in three lanes of a 3-8% Tris-Acetate gel (NuPAGE, Thermo Fisher Scientific), and stained with Coomassie-blue. The gel region corresponding to cross-linked complexes was sliced and digested overnight with trypsin to generate cross-linked peptides. After digestion, the peptide mixture was acidified and extracted from the gel as previously described (*31*, *32*). Peptides were fractionated offline by high pH reverse-phase chromatography, loaded onto an EASY-Spray column (Thermo Fisher Scientific ES800: 15 cm × 75 µm ID,

PepMap C18, 3 μm) via an EASY-nLC 1000, and gradient-eluted for online ESI-MS and MS/MS analyses with a Q Exactive Plus mass spectrometer (Thermo Fisher Scientific). MS/MS analyses of the top 8 precursors in each full scan used the following parameters: resolution: 17,500 (at 200 Th); AGC target: 2×10^5; maximum injection time: 800 ms; isolation width: 1.4 m/z; normalized collision energy: 24%; charge: 3–7; intensity threshold: 2.5×10^3; peptide match: off; dynamic exclusion tolerance: 1,500 mmu. Cross-linked peptides were identified from mass spectra by pLink (*33*). All spectra reported here were manually verified as previously (*31*).

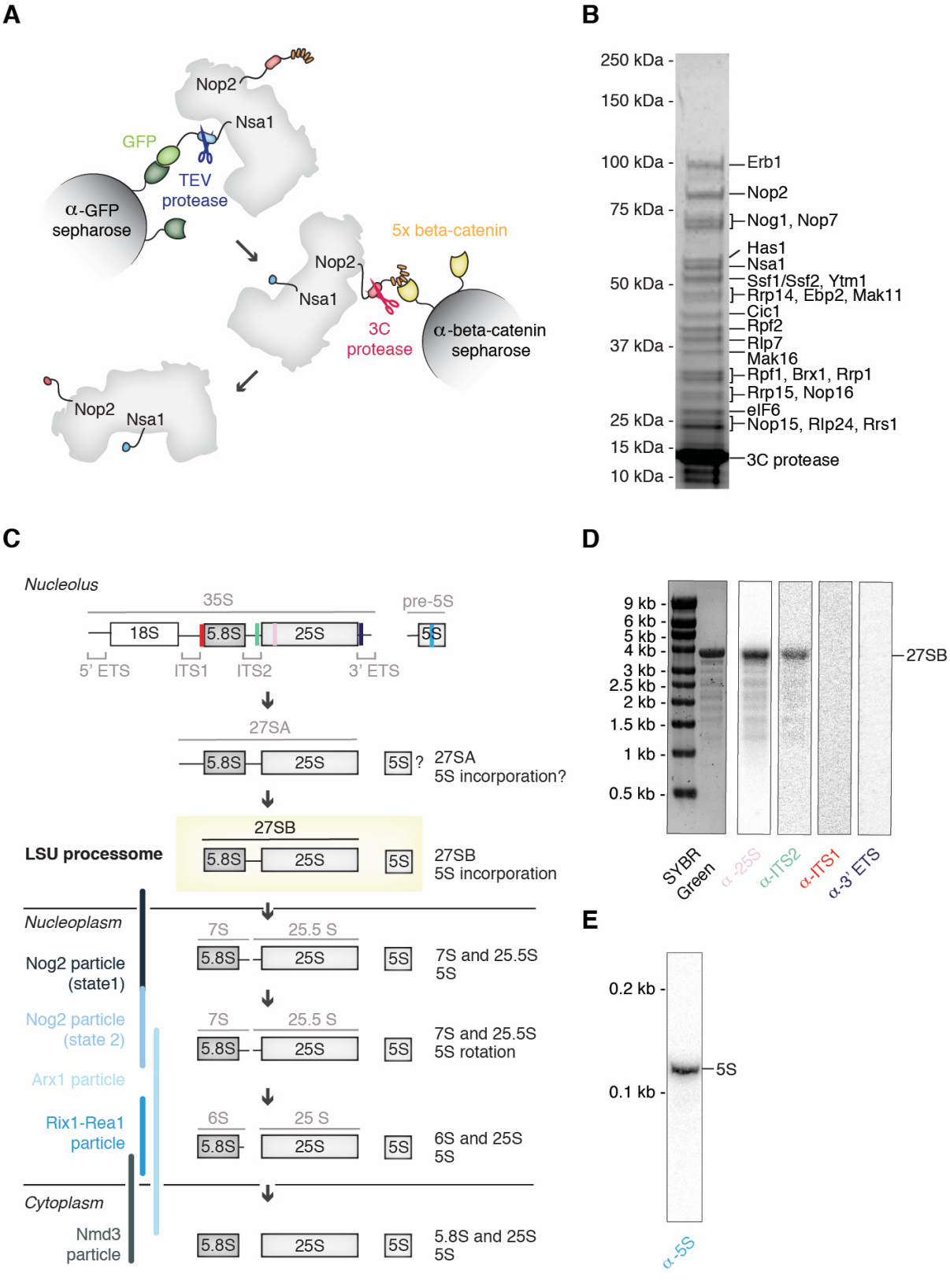
A
Nop2
Nsa1
GFP
TEV protease
α-GFP sepharose
5x beta-catenin
Nop2
Nsa1
3C protease
α-beta-catenin sepharose
Nop2
Nsa1
B
250 kDa
150 kDa
100 kDa
75 kDa
50 kDa
37 kDa
25 kDa
15 kDa
10 kDa
Erb1
Nop2
Nog1, Nop7
Has1
Nsa1
Ssf1/Ssf2, Ytm1
Rrp14, Ebp2, Mak11
Cic1
Rpf2
Rlp7
Mak16
Rpf1, Brx1, Rrp1
Rrp15, Nop16
eIF6
Nop15, Rlp24, Rrs1
3C protease
C
Nucleolus
35S
pre-5S
18S
5.8S
25S
5S
5' ETS
ITS1
ITS2
3' ETS
27SA
27SA
5S incorporation?
27SB
LSU processome
27SB
5S incorporation
Nucleoplasm
7S
25.5 S
Nog2 particle (state1)
7S and 25.5S
5S
Nog2 particle (state 2)
7S and 25.5S
5S rotation
Arx1 particle
Rix1-Rea1 particle
6S
25 S
6S and 25S
5S
Cytoplasm
Nmd3 particle
5.8S and 25S
5S
D
9 kb
6 kb
5 kb
4 kb
3 kb
2.5 kb
2 kb
1.5 kb
1 kb
0.5 kb
27SB
SYBR Green
α-25S
α-ITS2
α-ITS1
α-3' ETS
E
0.2 kb
0.1 kb
5S
α-5S

Fig. S1. **Purification of Nsa1/Nop2 tagged LSU processomes and analysis of RNA components.** (**A**) Schematic of tandem-affinity purification for the LSU processome from a yeast strain with a protease-cleavable GFP on Nsa1, and a 3C-protease cleavable 5x-beta-catenin peptide on Nop2. (**B**) Coomassie-blue stained SDS-PAGE of LSU particles purified as in (A). Protein labels are based on in solution mass-spectrometry analysis of purified LSU processome particles and the approximate molecular weight of each protein. (**C**) Schematic of rRNA processing for the large subunit in yeast. The RNA species contained in the LSU processome isolated in this work is boxed in yellow. The approximate residence times of the previously published pre-60S particles (the Nog2 particles, (*2*), the Arx1 particle (*34*), the Rix1-Rea1 particle (*3*) and the Nmd3 particle (*4*)) are highlighted by blue bars. The location of Northern blot probes are indicated by colored bars on the 35S and pre-5S transcript. (**D**) RNA isolated from the purified LSU processome was visualized on an agarose gel and stained using SYBR-green II. RNA separated on this gel was transferred onto a membrane and Northern blot analysis for the 25S, ITS2, ITS1 and 3' ETS RNAs was performed. (**E**) Isolated RNA was also visualized on a Urea-PAGE (not shown) and transferred onto a membrane and subjected to Northern blot analysis to test for the presence of the 5S rRNA.

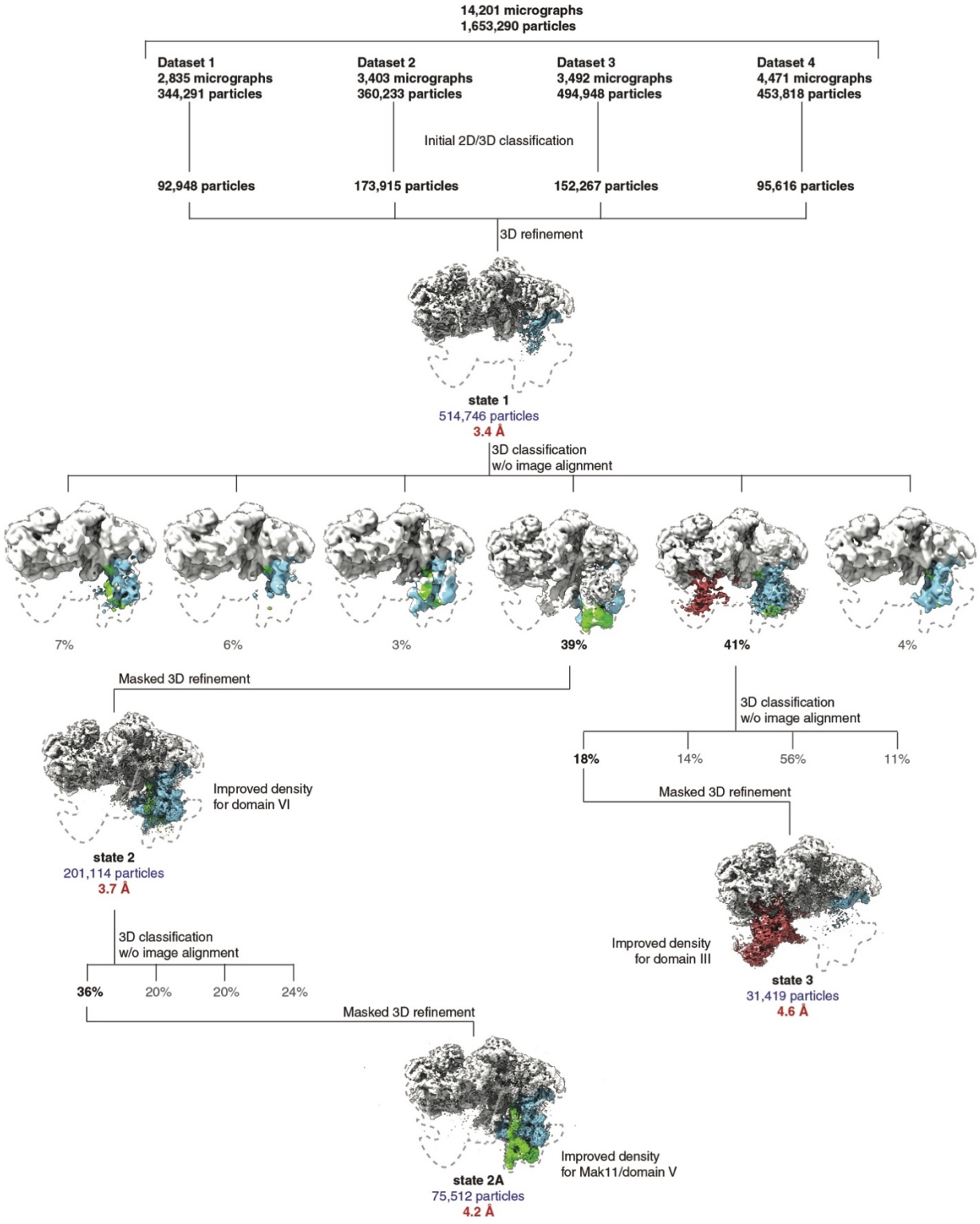
14,201 micrographs
1,653,290 particles
Dataset 1
2,835 micrographs
344,291 particles
Dataset 2
3,403 micrographs
360,233 particles
Dataset 3
3,492 micrographs
494,948 particles
Dataset 4
4,471 micrographs
453,818 particles
Initial 2D/3D classification
92,948 particles
173,915 particles
152,267 particles
95,616 particles
3D refinement
state 1
514,746 particles
3.4 Å
3D classification
w/o image alignment
7%
6%
3%
39%
41%
4%
Masked 3D refinement
Improved density
for domain VI
state 2
201,114 particles
3.7 Å
3D classification
w/o image alignment
36%
20%
20%
24%
Masked 3D refinement
Improved density
for Mak11/domain V
state 2A
75,512 particles
4.2 Å
3D classification
w/o image alignment
18%
14%
56%
11%
Masked 3D refinement
Improved density
for domain III
state 3
31,419 particles
4.6 Å

Fig. S2. Cryo-EM data-processing workflow. 14,201 micrographs were obtained over four data collections. These micrographs were aligned using MotionCor2 (*20*) with dose weighting, and imported into Relion2.1 (*22*) for further processing. After autopicking, manual cleaning of autopicked particles and sorting using 2D and 3D classification produced a total of 514,746 good particles. These particles were refined to produce the state 1 map, and further classified using a combination of focused 3D classification without alignment in order to obtain the state 2, state 2A and state 3 maps. Density regions corresponding to domain III (red), domain VI (blue) and Mak11 (green) are colored.

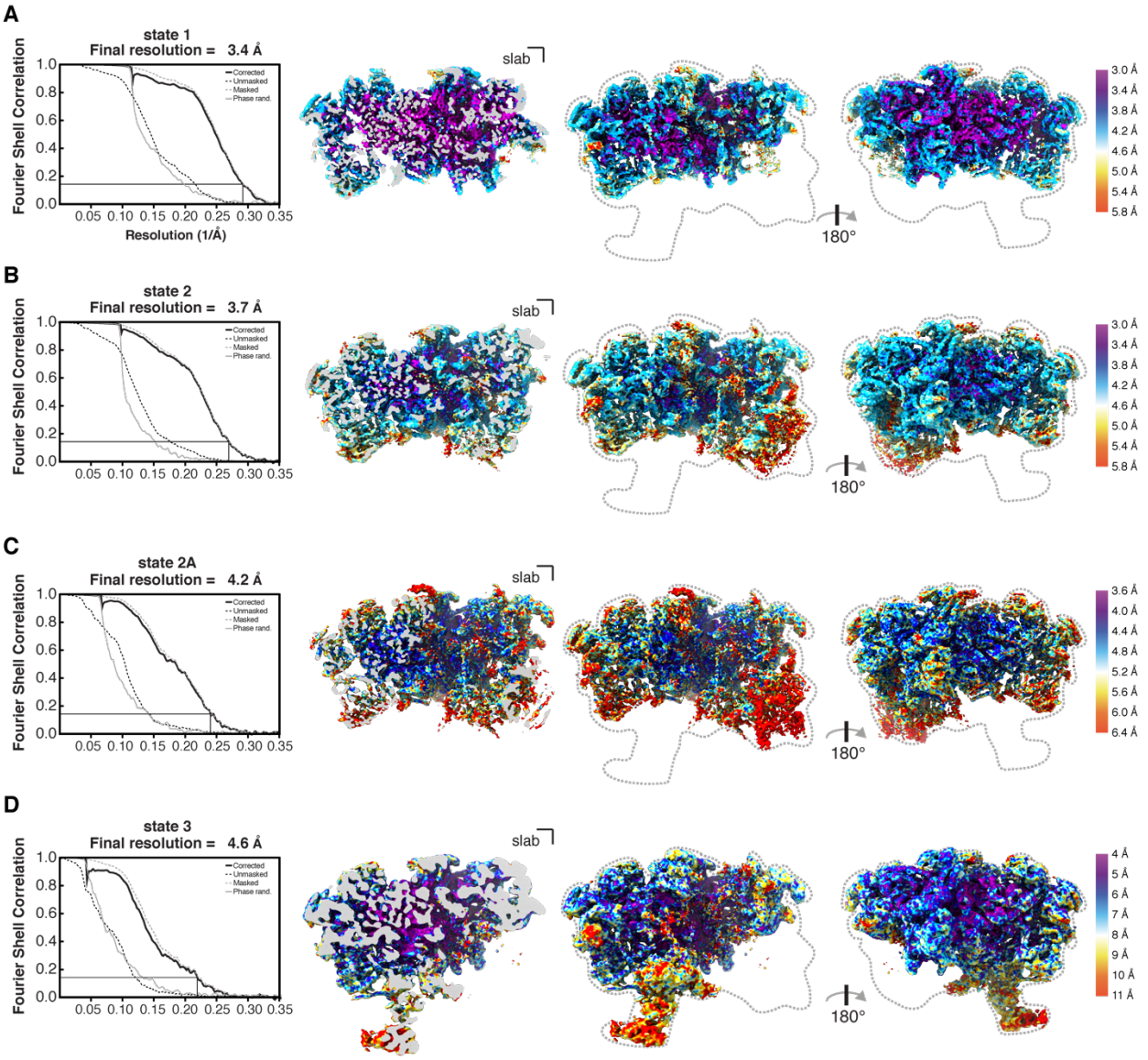

Fig. S3. Overall and local resolution estimates for state 1-3 cryo-EM maps. Overall and local resolution of **(A)** state 1 map at 3.4 Å, (**B**) the state 2 map at 3.7 Å, (**C**) the state 2A map with additional density for Mak11 at 4.2 Å, (**D**) the state 3 map at 6.1 Å. (**A-D)** The left panel shows Fourier Shell Correlation (FSC) curves for the unmasked (dashed black line), phase-randomized (solid grey line), the masked (dashed grey line) and the corrected map (solid black line). A thin black line indicates an FSC value of 0.143. A clipped view is shown next to two views of the obtained cryo-EM maps. The density volumes are colored according to local resolution using Resmap (*24*).

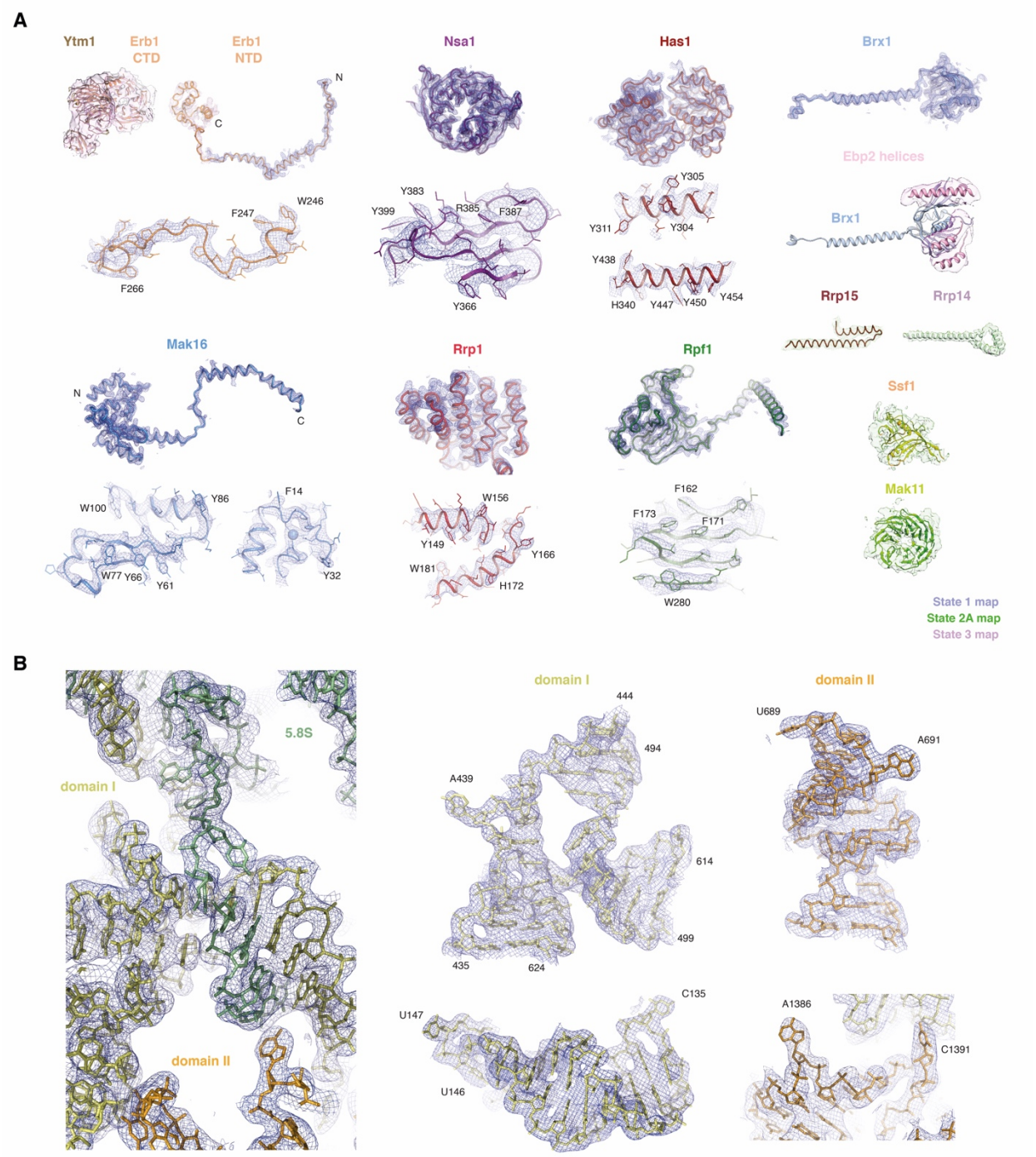

Fig. S4. **Cryo-EM density fit of selected LSU processome proteins and RNA models.** (**A**) Near atomic models of assembly factors are superimposed with their cryo-EM density. Images generated in PyMOL or Chimera. (**B**) Selected region of the 25S rRNA and 5.8S rRNA models superimposed with their cryo-EM density. Images generated in PyMOL.

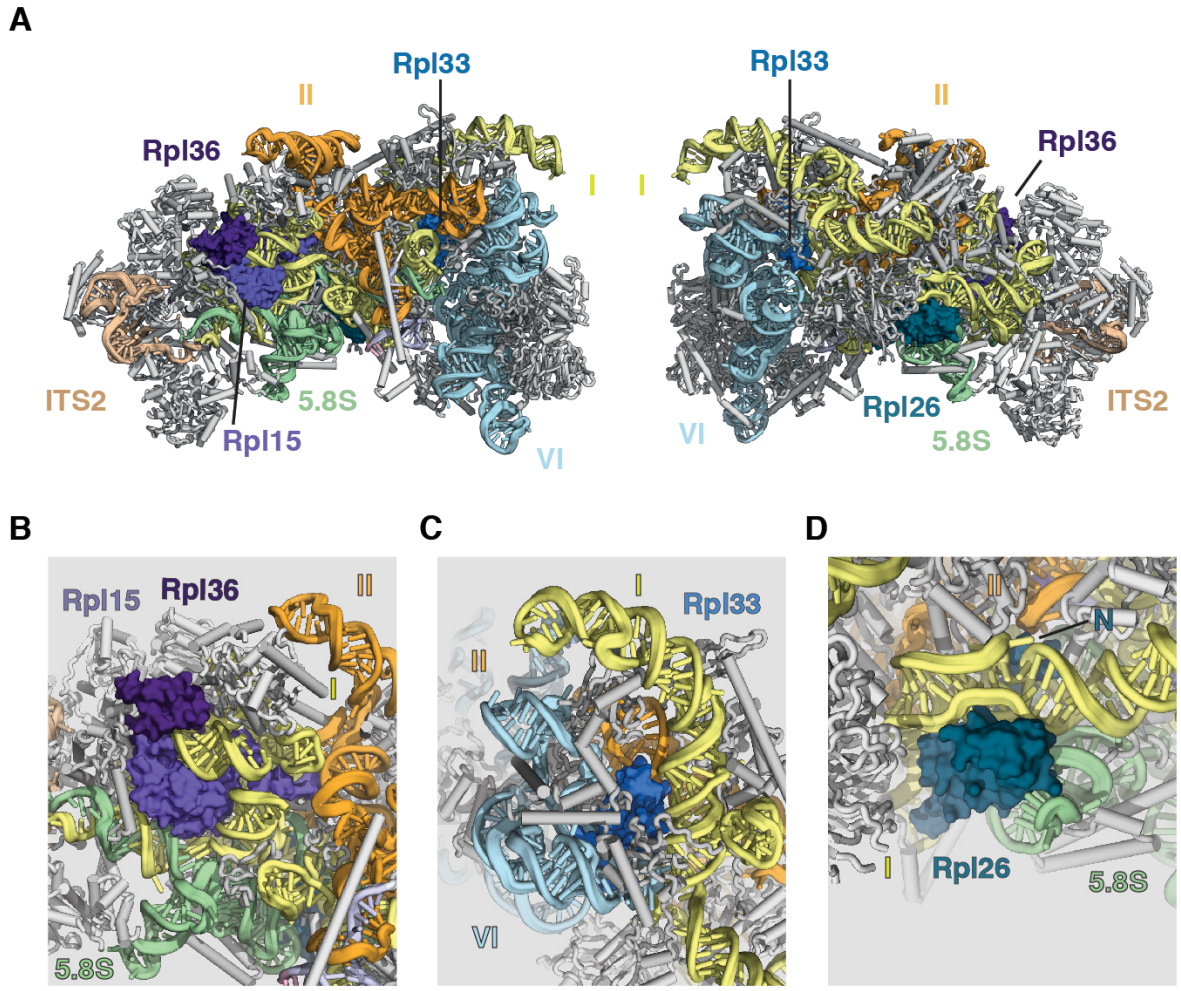

Fig. S5. Ribosomal proteins associated with Diamond-Blackfan anemia are positioned at rRNA domain junctions in the LSU processome. (**A**) Two views of the LSU processome state 2 model, with Diamond-Blackfan anemia associated ribosomal proteins shown in surface representation. (**B**) Rpl15 is located between the 5.8S-domain I duplex and a domain I-domain II interface. (**C**) Rpl33 (Rpl35 in *H. sapiens*) binds at the domain I, II, and VI junction of the 25S rRNA. (**D**) Rpl26 associates with the domain I -5.8S rRNA interface and additionally inserts its N-terminus (N) between domain I and II.

Table S1. Cryo-EM data collection parameters and refinement and validation statistics.

	State 1	State 2	State 2A	State 3
Data collection and processing				
Magnification	22,500X			
Voltage (kV)	300			
Pixel size (Å)	1.3			
Electron exposure (e- / Å^2)	47			
Defocus range (um)	1.0-3.5			
Symmetry imposed	C1			
Initial particle images	1,653,290			
Final particle images	514,746	201,114	75,512	31,419
Resolution (Å)	3.4	3.7	4.2	4.6
FSC threshold	0.143			
Map sharpening B-Factor (Å^2)	-68.7	-71.7	-83.0	-94.2
Refinement				
Model composition				
Non hydrogen atoms	91,570			
Protein residues	7126			
RNA bases	1606			
Ligands	2			
R.m.s. deviations				
Bond length (Å)	0.007			
Angles (°)	1.08			
Validation				
MolProbity score	2.12			
Clashscore	12.56			
Rotamer outliers (%)	0.48			
Good sugar puckers (%)	97.8			
Ramachandran				
Favored (%)	91.26			
Allowed (%)	8.27			
Outliers (%)	0.48			

Table S2. Molecular models of the LSU processome. Individual protein chains are listed with their initial PDB template (if not built *de novo*) and the LSU processome state(s) in which they are present.

Subgroup	Chain ID	SegID	Molecule name	Initial PDB template	Present in…
RNA	1	L2	25S	3JCT	All states
	2	L2	5.8S	3JCT	All states
	6	L6	ITS2	3JCT	All states
	3	L3	Magnesium		All states
Ribosomal proteins	C	ALC	Rpl4A_uL4	3JCT	All states
	E	ALE	Rpl6A_eL6	3JCT	All states
	e	ASE	Rpl32_eL32	3JCT	All states
	F	ALF	Rpl7A_uL30	3JCT	All states
	f	ASF	Rpl33A_eL33	3JCT	All states
	G	ALG	Rpl8A_eL8	3JCT	All states
	h	ASH	Rpl35A_uL29	3JCT	All states
	i	ASI	Rpl36A_eL36	3JCT	All states
	L	ALL	Rpl13A_eL13	3JCT	All states
	M	ALM	Rpl14A_eL14	3JCT	All states
	N	ALN	Rpl15A_eL15	3JCT	All states
	O	BLO	Rpl16A_uL13	3JCT	All states
	Q	ALQ	Rpl18A_eL18	4v88	All states
	S	ALS	Rpl20A_eL20	3JCT	All states
	B	BLB	Rpl3_uL3	4v88, chain DB	State 2
	P	BLP	Rpl17A_uL22	3JCT	State 2
	V	BLV	Rpl23A_uL14	3JCT	State 2
	Y	ALY	Rpl26A_uL26	3JCT	All states
	j	ASJ	Rpl37_eL37	3JCT	All states
	Z	CLZ	Rpl27A_eL27	3JCT	State 3
	k	CSK	Rpl38_eL38	3JCT	State 3
	g	CSG	Rpl34A_eL34	3JCT	State 3
	c	CSC	Rpl30_eL30	3JCT	State 3
	X	CLX	Rpl25_uL23	3JCT	State 3
Assembly factors in Nog2	K	ALK	Cic1	3JCT	All states
	n	ASN	Nop7 (PESC)	3JCT	All states
	o	ASO	Nop15	3JCT	All states
	t	AST	Rlp7	3JCT	All states
	u	BSU	Rlp24	3JCT	State 2
	y	BSY	Tif6	3JCT	State 2
	W	BLW	Nog1	Manual building	State 2
New assembly factors	A	ALA	Nsa1	5SUI	All states
	p	ASP	Has1	Phyre model based on 2V1X	All states
	b	ASB	Brx1	Model based on 5WLC, chain SM	All states
	m	ASM	Ebp2	De novo	All states
	z	ASZ	Rrp1	De novo	All states
	D	ALD	Mak16	De novo	All states
	I	ALI	Rpf1	Phyre model based on 5JPQ, chain c	All states
	s	ASS	Erb1-NTD	De novo	All states
	w	BSW	Rrp15	De novo	State 2
	v	BSV	Ssf1	Phyre model based on 4XV9	State 2
	q	BSQ	Mak11	Phyre model based on 3DM0	States 2 and 2A
	s	CSS	Erb1-CTD	5CXB	State 3
	d	CSD	Ytm1	5CXB	State 3
	7	AS7	Nop16	De novo	All states
	8	BS8	Rrp14	De novo	State 2

Data Table S1 (separate file). DSS cross-links for the LSU processome.

Data File S1. PyMOL script for the structural analysis of the LSU processome.

Movie S1. 360° view of the cryo-EM reconstruction of the *S. cerevisiae* LSU processome. A 360° rotation of a composite cryo-EM map consisting of the 3.4 Å state1 and the 3.7 Å state 2 maps. Densities for LSU processome assembly factors and rRNA domains are color-coded as in Fig. 1 and ribosomal proteins are colored in grey. The rotation is paused at front and back view as shown in Fig. 1.

Supplementary References:

18. M. B. Braun *et al.*, Peptides in headlock--a novel high-affinity and versatile peptide-binding nanobody for proteomics and microscopy. *Sci Rep*. **6**, 19211 (2016).

19. D. N. Mastronarde, Automated electron microscope tomography using robust prediction of specimen movements. *J. Struct. Biol.* **152**, 36–51 (2005).

20. S. Q. Zheng *et al.*, MotionCor2: anisotropic correction of beam-induced motion for improved cryo-electron microscopy. *Nat. Methods*. **14**, 331–332 (2017).

21. A. Rohou, N. Grigorieff, CTFFIND4: Fast and accurate defocus estimation from electron micrographs. *J. Struct. Biol.* **192**, 216–221 (2015).

22. D. Kimanius, B. O. Forsberg, S. H. Scheres, E. Lindahl, Accelerated cryo-EM structure determination with parallelisation using GPUs in RELION-2. *Elife*. **5**, 19 (2016).

23. A. Punjani, J. L. Rubinstein, D. J. Fleet, M. A. Brubaker, cryoSPARC: algorithms for rapid unsupervised cryo-EM structure determination. *Nat. Methods*. **14**, 290–296 (2017).

24. A. Kucukelbir, F. J. Sigworth, H. D. Tagare, Quantifying the local resolution of cryo-EM density maps. *Nat. Methods*. **11**, 63–65 (2014).

25. Y.-H. Lo, E. M. Romes, M. C. Pillon, M. Sobhany, R. E. Stanley, Structural Analysis Reveals Features of Ribosome Assembly Factor Nsa1/WDR74 Important for Localization and Interaction with Rix7/NVL2. *Structure*. **25**, 762–772.e4 (2017).

26. M. Wegrecki, O. Rodríguez-Galán, J. de la Cruz, J. Bravo, The structure of Erb1-Ytm1 complex reveals the functional importance of a high-affinity binding between two β-propellers during the assembly of large ribosomal subunits in eukaryotes.

Nucleic Acids Research, **43** 11017-30 (2015).

27. L. A. Kelley, S. Mezulis, C. M. Yates, M. N. Wass, M. J. E. Sternberg, The Phyre2 web portal for protein modeling, prediction and analysis. *Nat Protoc*. **10**, 845–858 (2015).

28. P. Emsley, K. Cowtan, Coot: model-building tools for molecular graphics. *Acta Crystallogr. D Biol. Crystallogr.* **60**, 2126–2132 (2004).

29. P. D. Adams *et al*., PHENIX: a comprehensive Python-based system for macromolecular structure solution. *Acta Crystallogr. D Biol. Crystallogr.* **66**, 213–221 (2010).

30. E. F. Pettersen *et al*., UCSF Chimera--a visualization system for exploratory research and analysis. *J Comput Chem*. **25**, 1605–1612 (2004).

31. Y. Shi *et al*., Structural characterization by cross-linking reveals the detailed architecture of a coatomer-related heptameric module from the nuclear pore complex. *Mol. Cell Proteomics*. **13**, 2927–2943 (2014).

32. Y. Shi *et al*., A strategy for dissecting the architectures of native macromolecular assemblies. *Nat. Methods*. **12**, 1135–1138 (2015).

33. B. Yang *et al*., Identification of cross-linked peptides from complex samples. *Nat. Methods*. **9**, 904–906 (2012).

34. B. Bradatsch *et al*., Structure of the pre-60S ribosomal subunit with nuclear export factor Arx1 bound at the exit tunnel. *Nat. Struct. Mol. Biol.* **19**, 1234–1241 (2012).